

Center for Quality and Applied Statistics
Kate Gleason College of Engineering
Rochester Institute of Technology

Analytical Treatment of Detection Power in Simulated Hyperspectral Images

Peter Bajorski
Center for Quality and Applied Statistics
Rochester Institute of Technology
Peter.Bajorski@rit.edu

Technical Report 2005–5

June 2005



Analytical Treatment of Detection Power in Simulated Hyperspectral Images

Peter Bajorski

Graduate Statistics Department
Rochester Institute of Technology
98 Lomb Memorial Drive
Rochester, NY, USA
Email: Peter.Bajorski@rit.edu

Abstract—This paper describes continuation of recent research on analytical treatment of detection power of subpixel target detectors. In previous papers, we showed that the detection power of the OSP detector is negatively influenced by a small angle between the target signature and the background subspace. On the other hand, the MFD detector is not impacted by this angle. However, the MFD is adversely impacted by its bias. The relative performance of the OSP versus MFD will depend on the balance of these two “forces” influencing performance of these detectors. In this paper, we consider uniform distributions (often used in simulations) of the abundances of the background signatures, and derive formulas for detection power of the OSP and MFD detectors. We show three numerical examples of the balance between the bias of MFD and the large variability of OSP and its impact on the relative performance of these detectors.

Keywords: *hyperspectral image, subpixel target detection, orthogonal subspace projection, matched filter detector, detection power.*

I. INTRODUCTION

This paper describes continuation of recent research on analytical treatment of detection power of the subpixel target detectors. In previous papers ([1] and [2]), we showed that the detection power of the OSP detector is negatively influenced by its increased variability caused by a small angle between the target signature and the background subspace. On the other hand, the MFD detector is not impacted by this angle. However, the MFD is adversely impacted by its bias, which depends on the distribution of background signatures in the target and non-target pixel spectra. The resulting relative performance of the OSP versus MFD will depend on the balance of the two “forces” influencing performance of these detectors.

The purpose of this paper is to investigate the case of uniform distributions of the abundances of the background signatures. Such distributions are sometimes used in simulations of hyperspectral images [3].

Section II introduces the notation and gives the formulation of the model used in this paper. Section III provides the main results on the analytical formulas for the detection power of MFD and OSP detectors. Section IV shows three numerical examples of the balance between the bias of MFD and the large variability of OSP and its impact on the relative performance of these detectors. The Appendix gives some probabilistic results needed for the main theoretical results of Section III.

II. MODEL FORMULATION

Consider a set of image spectra $\mathbf{r}_i, i = 1, \dots, n$, where \mathbf{r}_i 's are p -dimensional vectors (of reflectance or radiance, for example). For the purpose of target detection, the following structured model is often used in literature ([4], [5], [6], [7], [8], [9])

$$\mathbf{r}_i = \mathbf{d} \cdot \theta_i + \mathbf{U} \cdot \boldsymbol{\gamma}_i + \boldsymbol{\varepsilon}_i \quad (1)$$

where \mathbf{d} is a fixed known vector of the target spectrum, \mathbf{U} is a fixed known matrix of background spectra as columns, and θ_i , $\boldsymbol{\gamma}_i$ are unknown constant and vector of abundances, respectively. The error term $\boldsymbol{\varepsilon}_i$ is assumed to follow the multivariate normal (Gaussian) distribution $N(\mathbf{0}, \sigma^2 \mathbf{I})$.

The target detection problem can be formulated as a hypothesis-testing problem as follows. The null hypothesis H_0 means that the target signature \mathbf{d} is not present in a given spectra, and the alternative hypothesis H_1 means that the target signature \mathbf{d} is present. In [2], we introduced the following general description of these hypotheses in order to account for the variability of material abundances within the whole image (set of spectra).

For a p -dimensional spectrum vector \mathbf{r} :

$$H_0 : \mathbf{r} = \mathbf{U} \cdot \boldsymbol{\gamma} + \boldsymbol{\varepsilon}$$

$$H_1 : \mathbf{r} = \mathbf{d} \cdot \theta + \mathbf{U} \cdot \boldsymbol{\gamma} + \boldsymbol{\varepsilon}$$

where $\boldsymbol{\gamma}$ and $(\theta, \boldsymbol{\gamma})$ are random vectors describing the variability of abundances within the whole set of spectra, and the error term $\boldsymbol{\varepsilon}$ represents the joint effect of the noise in data and possible error in modeling.

In this paper, we assume that $\boldsymbol{\varepsilon}$ follows the multivariate normal (Gaussian) distribution $N(\mathbf{0}, \sigma^2 \mathbf{I})$ and is stochastically independent of the random vectors $\boldsymbol{\gamma}$ and $(\theta, \boldsymbol{\gamma})$. We also assume that \mathbf{U} consists of two background spectra, so consequently the random vector $\boldsymbol{\gamma}$ consists of two coordinates (γ_1, γ_2) . Then we assume the following distribution of abundances under the two hypotheses:

(γ_1, γ_2) is uniformly distributed on S_2 under H_0

$(\theta, \gamma_1, \gamma_2)$ is uniformly distributed on S_3 under H_1

where S_k is a simplex defined as

$$S_k = \left\{ \mathbf{x} = (x_1, \dots, x_k) : x_i \geq 0 \text{ for } i = 1, \dots, k \text{ and } \sum_{i=1}^k x_i = 1 \right\}$$

The purpose of this paper is to compare the performance of the matched filter detector (MFD) defined as

$$D_{MFD}(\mathbf{r}) = \frac{\mathbf{d}^T \mathbf{r}}{\mathbf{d}^T \mathbf{d}}$$

with that of the orthogonal subspace projection (OSP) detector defined as

$$D_{OSP}(\mathbf{r}) = \frac{\mathbf{d}^T P_U^\perp \mathbf{r}}{\mathbf{d}^T P_U^\perp \mathbf{d}}. \quad (3)$$

In [1], we showed that for fixed values of the abundance coefficients θ_i and γ_i under the model (1),

$$D_{MFD}(\mathbf{r}) \sim N\left(\theta_i + \mathbf{a}^T \gamma_i, (\mathbf{d}^T \mathbf{d})^{-1} \sigma^2\right)$$

and

$$D_{OSP}(\mathbf{r}) \sim N\left(\theta_i, (\mathbf{d}^T P_U^\perp \mathbf{d})^{-1} \sigma^2\right)$$

where $\mathbf{a}^T = (\mathbf{d}^T \mathbf{d})^{-1} \mathbf{d}^T \mathbf{U}$. In this paper, we treat these results as conditional, given specific realizations of the random vectors γ and (θ, γ) .

III. THEORETICAL RESULTS

We now formulate two theorems about the detection power of the MFD and OSP detectors.

Theorem 1. Under the hypotheses defined in (2), the detection power of MFD is given by

$$P_{MFD, \alpha} = \begin{cases} 1 - F_3(b_2 + q_1(1 - \alpha, b_1), b_1, b_2) & \text{when } b_1 \cdot b_2 > 0 \\ 1 - F_3(b_2 + q_1(1 - \alpha, b_1) - b_1, b_2 - b_1, -b_1) & \text{when } b_1 < 0 \text{ and } b_2 > 0 \end{cases}$$

where $b_i = \frac{a_i - 1}{\sigma} \sqrt{\mathbf{d}^T \mathbf{d}}$ for $i = 1, 2$, $\mathbf{a}^T = [a_1, a_2]$,

$q_1(1 - \alpha, b_1)$ is the $(1 - \alpha)$ quantile (percentile) from the F_1 distribution defined in the appendix ($b_1 = k_1$), and F_3 is a CDF of another distribution defined in the Appendix.

Theorem 2. Under the hypotheses defined in (2), the detection power of OSP is given by

$$P_{OSP, \alpha} = 1 - F_2\left(z_{1-\alpha}, \frac{\sqrt{\mathbf{d}^T P_U^\perp \mathbf{d}}}{\sigma}\right),$$

where $z_{1-\alpha}$ is the $(1 - \alpha)$ percentile from the standard normal (Gaussian) distribution, and F_2 is a CDF defined in the Appendix.

The proofs of both theorems consist of some extensive calculus and algebra and are outlined in the Appendix.

IV. NUMERICAL RESULTS

We now show some numerical results for the three material spectra used in [3] (and also in [1]). We consider the following three cases:

1. Barite is considered the target material, when two other materials (chalcopyrite and pyrite) are used as background materials.
2. Chalcopyrite is considered the target material, when two other materials (barite and pyrite) are used as background materials.
3. Pyrite is considered the target material, when two other materials (barite and chalcopyrite) are used as background materials.

In all three cases, σ is chosen so that $\sqrt{\mathbf{d}^T \mathbf{d}} / \sigma = \sqrt{10^{2.5}}$ (to make it consistent with previous examples in [1] and [3], where $\mathbf{d}^T \mathbf{d} / \sigma^2$ was assumed to be 25 dB).

Figures 1 through 3 show detection power of the MFD and OSP detectors as functions of the false alarm rate in a range from 0 to 0.1 for Cases 1 through 3, respectively.

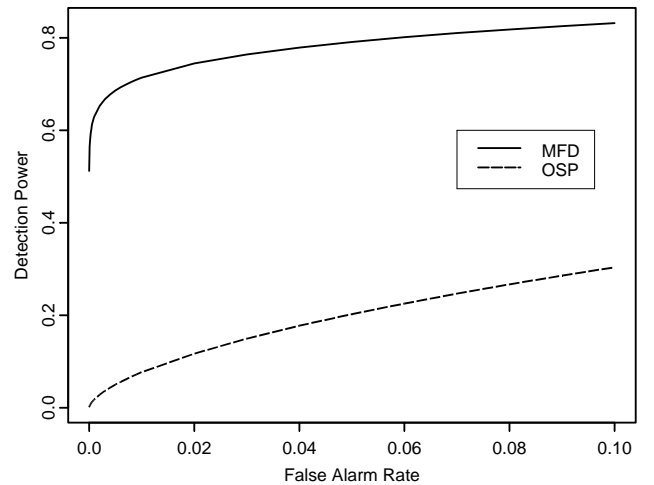


Figure 1. Detection power of the MFD and OSP detectors as functions of the false alarm rate, when barite is considered the target material, and two other materials (chalcopyrite and pyrite) are used as background materials

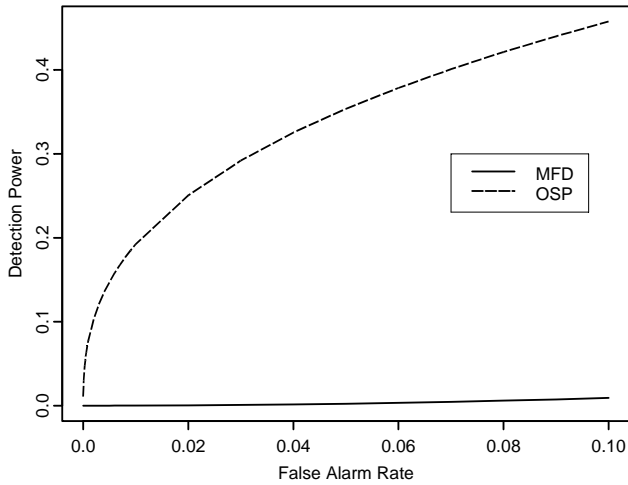


Figure 2. Detection power of the MFD and OSP detectors as functions of the false alarm rate, when chalcopyrite is considered the target material, and two other materials (barite and pyrite) are used as background materials

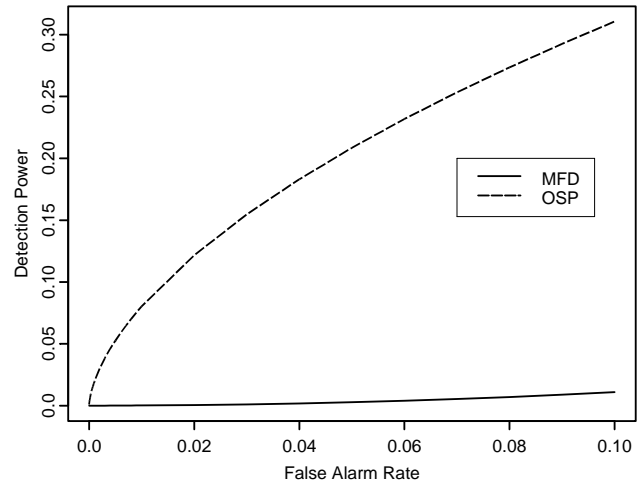


Figure 3. Detection power of the MFD and OSP detectors as functions of the false alarm rate, when pyrite is considered the target material, and two other materials (barite and chalcopyrite) are used as background materials

Figures 1 through 3 demonstrate that MFD may outperform OSP in some cases, while it may be inferior in some other cases. The following table shows the role of the bias vector $\mathbf{a}^T = [a_1, a_2]$ and the angle ω between \mathbf{d} and the subspace $\langle \mathbf{U} \rangle$ generated by column vectors of \mathbf{U} . The quantity

$$\frac{1}{\sin(\omega)} = \frac{\sqrt{\mathbf{d}^T \mathbf{d}}}{\sqrt{\mathbf{d}^T P_{\mathbf{U}}^{\perp} \mathbf{d}}}$$

measures how many times the variability (standard deviation) of OSP is larger than that of MFD in (4).

TABLE I. THE NUMERICAL VALUES OF PARAMETERS HAVING AN IMPACT ON THE RELATIVE PERFORMANCE OF MFD VERSUS OSP

	a_1	a_2	Angle ω in degrees	$\frac{1}{\sin(\omega)}$
Case 1	0.09	0.16	6.9	8.3
Case 2	10.47	1.67	11.5	5.1
Case 3	6.22	0.57	7.1	8.1

We can see that the variability of the OSP statistic is much larger than that of MFD in all three cases, which favors MFD. In Case 1, the biasing constants a_1 and a_2 are very small, so the impact on MFD is minimal, and MFD dominates OSP in detection power. In Cases 2 and 3, the biasing constants are much larger, which is very detrimental to the MFD performance. These three cases give a good example of how the balance between the bias of MFD and the large variability of OSP impacts the relative performance of these detectors.

V. APPENDIX

Let us introduce the following notation:

$$\phi(x) = \frac{1}{\sqrt{2\pi}} \exp\left(-\frac{x^2}{2}\right)$$

is the PDF (probability density function) of the standard normal distribution $N(0,1)$

$$\Phi(x) = \int_{-\infty}^x \phi(t) dt$$

is the CDF (cumulative distribution function) of the standard normal distribution $N(0,1)$

$$H(x) = \int_{-\infty}^x \Phi(t) dt = x\Phi(x) + \phi(x)$$

$$G(x) = \int_{-\infty}^x H(t) dt = \frac{1}{2} [xH(x) + \Phi(x)]$$

$$M_h(x) = H(x) - H(x-h)$$

$$L_h(x) = G(x) - G(x-h)$$

Let us assume that a random variable Z_0 follows a normal distribution $N(0,1)$, and k and m are positive real numbers such that $k > m$. Also assume that

X_1 follows a uniform distribution on the interval $(0, k)$;

X_2 follows a triangular distribution with the density function given by

$$g_2(x) = \begin{cases} \frac{2}{k^2}(k-x) & \text{for } 0 < x < k \\ 0 & \text{otherwise} \end{cases}$$

X_3 follows a triangular distribution with the density function given by

$$g_3(x) = \begin{cases} \frac{2}{mk}x & \text{for } 0 < x < m \\ \frac{2}{k(k-m)}(k-x) & \text{for } m < x < k \\ 0 & \text{otherwise} \end{cases}$$

Define $Y_i = X_i + Z_0$ for $i = 1, 2$, and 3 .

Lemma 1. The CDF F_1 of Y_1 is given by

$$F_1(x; k) = \frac{1}{k} [H(x) - H(x - k)]$$

Lemma 2. The CDF F_2 of Y_2 is given by

$$F_2(x; k) = \frac{2}{k} \left[H(x) - \frac{1}{k} L_k(x) \right]$$

Lemma 3. The CDF F_3 of Y_3 is given by

$$F_3(x; k, m) = \frac{2}{k} \left[\frac{1}{m} L_m(x) - \frac{1}{k-m} L_{(k-m)}(x-m) \right]$$

Proof of Theorem 1: Based on (4), $D_{MFD}(\mathbf{r})$ is distributed as

$$\theta + \mathbf{a}^T \boldsymbol{\gamma} + Z,$$

where $Z \sim N\left(0, (\mathbf{d}^T \mathbf{d})^{-1} \sigma^2\right)$. Under H_0 in (2), $\theta = 0$

and $\gamma_2 = 1 - \gamma_1$, which leads to $\mathbf{a}^T \boldsymbol{\gamma} = a_2 + (a_1 - a_2)\gamma_1$. Finally, introducing $Z_0 \sim N(0, 1)$, $D_{MFD}(\mathbf{r})$ is distributed as

$$a_2 + \frac{\sigma}{\sqrt{\mathbf{d}^T \mathbf{d}}} \left[\frac{\sqrt{\mathbf{d}^T \mathbf{d}}}{\sigma} (a_1 - a_2) \gamma_1 + Z_0 \right],$$

which is distributed (based on Lemma 1) as

$$a_2 + \frac{\sigma}{\sqrt{\mathbf{d}^T \mathbf{d}}} Y_1$$

where Y_1 has the CDF F_1 with $k = \frac{\sqrt{\mathbf{d}^T \mathbf{d}}}{\sigma} (a_1 - a_2)$. Similar (but more extensive) calculations based on Lemma 3 give the distribution of $D_{MFD}(\mathbf{r})$ under H_1 , which then leads to the given formula for the detection power. \square

Proof of Theorem 2: This proof is based on Lemma 2 and it consists of calculations similar to those in the proof of Theorem 1. \square

REFERENCES

- [1] P. Bajorski, "Analytical Comparison of Subpixel Target Detectors in Structured Models for Hyperspectral Images," *Proc. SPIE, Algorithms and Technologies for Multispectral, Hyperspectral, and Ultraspectral Imagery XI*, Orlando, FL, March/April 2005.
- [2] P. Bajorski, "Impact of Material Abundances Distributions on Detection Power in Hyperspectral Images," *Proc. of IEEE International Geoscience and Remote Sensing Symposium, July 2005*.
- [3] S. Johnson, "Constrained energy minimization and the target-constrained interference-minimization filter," *Optical Engineering*, vol. 42, No. 6, pp. 1850–54, June 2003.
- [4] C.-I. Chang, X.-L. Zhao, M. L. G. Althouse, and J. J. Pan, "Least squares subspace projection approach to mixed pixel classification for hyperspectral images," *IEEE Trans. Geosci. Remote Sensing*, vol. 36, pp. 898–912, May 1998.
- [5] D. Manolakis and G. Shaw. Detection algorithms for hyperspectral imaging applications. *IEEE Signal Processing Magazine*, 19(1):29–43, January 2002.
- [6] L.L. Scharf, B. Friedlander, "Matched Subspace Detectors," *IEEE Trans. Signal Processing*, vol. 42, No. 8, pp. 2146–2156, August 1994.
- [7] S. Johnson, "The relationship between the matched filter operator and the target signature space orthogonal projection classifier," *IEEE Trans. Geosci. Remote Sensing*, vol. 38, pp. 283–286, Jan. 2000.
- [8] T. M. Tu, C.-H. Chen, and C.-I. Chang, "A least squares orthogonal subspace projection approach to desired signature extraction and detection," *IEEE Trans. Geosci. Remote Sensing*, vol. 35, pp. 127–139, Jan. 1997.
- [9] C.-I. Chang, *Hyperspectral Imaging: Techniques for Spectral Detection and Classification*, Kluwer Academic/Plenum Publishers, 2003.